ACS SENSORS

pubs.acs.org/acssensors

Article

Tandem Cas13a/crRNA-Mediated CRISPR-FET Biosensor: A One-for-All Check Station for Virus without Amplification

Jiahao Li, Lina Tang, Tingxian Li, Kun Li, Yulin Zhang, Wei Ni, Meng-Meng Xiao, Youyun Zhao,* Zhi-Yong Zhang,* and Guo-Jun Zhang*

Cite This: *ACS Sens.* 2022, 7, 2680−2690

Read Online

ACCESS | Metrics & More | Article Recommendations | Supporting Information

ABSTRACT: The path toward field-effect transistor (FET) application from laboratory to clinic has delivered a compelling push in the biomedical domain, yet ultrasensitive and timely pathogen identification without PCR remains a long-lasting challenge. Herein, we create a generic check station termed "CRISPR-FET", first incorporating the CRISPR/Cas13a system within the FET modality, for accelerated and unamplified detection of viral RNA. Unlike conventional FETs bearing target-specific receptors, this sensor holds three unique advancements: (i) an ingenious sensing mechanism is used, which converts the signal of a large-sized analyte into an on-chip cleavage response of an immobilized CRISPR reporter, enabling signal generation events to occur all within the Debye length; (ii) the multipurpose inspection of the CoV ORF1ab, CoV N gene, and HCV RNA unveils the potential for "one-for-all" scalable FET-based molecular diagnostics; and (iii) it is shown that Cas13a-crRNAs targeting different sites of the viral genome can be deployed in tandem to amplify the FET response, empowering the detection limit down to 1.56 aM, which is a world-record level of sensitivity in the FET for direct viral gene sensing. Notably, a brilliant clinical applicability was made in distinguishing HCV-infected patients from normal controls. Overall, this study sheds new insights into FET-based nucleic acid sensing technology and invokes a vision for its possible future roles in diagnosis of various viral diseases.

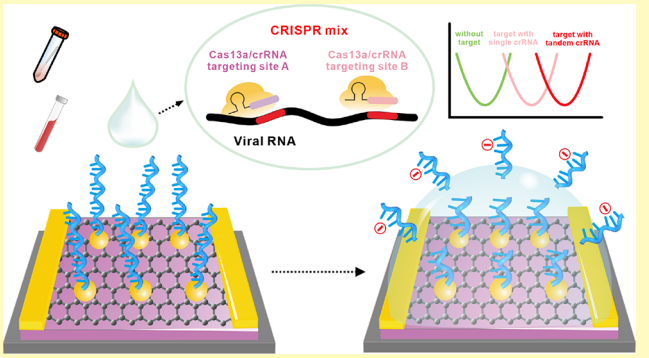

KEYWORDS: *CRISPR/Cas13, field-effect transistor, virus, detection, amplification-free*

INTRODUCTION

Infectious viral diseases, which have led to more than 2 million deaths worldwide annually, account for a large share of global morbidities and mortalities.[1] Some of these diseases caused by viruses, historically, such as Ebola virus (EboV), human immunodeficiency virus (HIV), coronavirus (CoV), and hepatitis C virus (HCV), to name a few, are highly pathogenic and contagious, having wreaked intimidating social threat and economic havoc. In previous and contemporary pandemics, one of the formidable challenges has been the availability of rapid and precise testing, especially in low-resource settings, which is beyond the reach of centralized clinical laboratory service. Among the diverse virus detection strategies, RT-PCR (reverse transcription-polymerase chain reaction) is an exemplary diagnostic tool with high sensitivity and accurate quantification. The limitations, however, appear with the need for expensive equipment, elaborated hardware, and high demand for well-trained operators, which inflict a sparse network of virus screening hubs that can adversely affect the scalability during an outbreak. Besides, a long turn-around time resulting from intricate sample manipulation and tedious thermal cycle process can bring about possible delays in pertinent diagnoses and increase the chances of widespread transmission. Therefore, one of the first priorities in resilience to viral pandemics is to develop new testing alternatives that can address PCR-related issues but without sacrificing PCR-like sensitivity.

In recent years, the CRISPR/Cas system has been advanced into a new generation of molecular diagnostic innovation, receiving increasing attention as a powerful weapon to combat viral infections.[2] Cas13, a member of class II type VI CRISPR effector proteins, including four subtypes (Cas13a−Cas13d) functions as a CRISPR RNA (crRNA)-guided RNA-targeting ribonuclease.[3,4] At present, CRISPR/Cas13 has been extensively employed for RNA detection. Briefly, upon actuation of target RNA, Cas13 is activated to engage in the cleavage of surrounding reporter RNAs (reRNA) linked with a fluoro-

Received: June 7, 2022
Accepted: August 29, 2022
Published: September 8, 2022

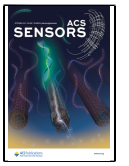

https://doi.org/10.1021/acssensors.2c01200
ACS Sens. 2022, 7, 2680−2690

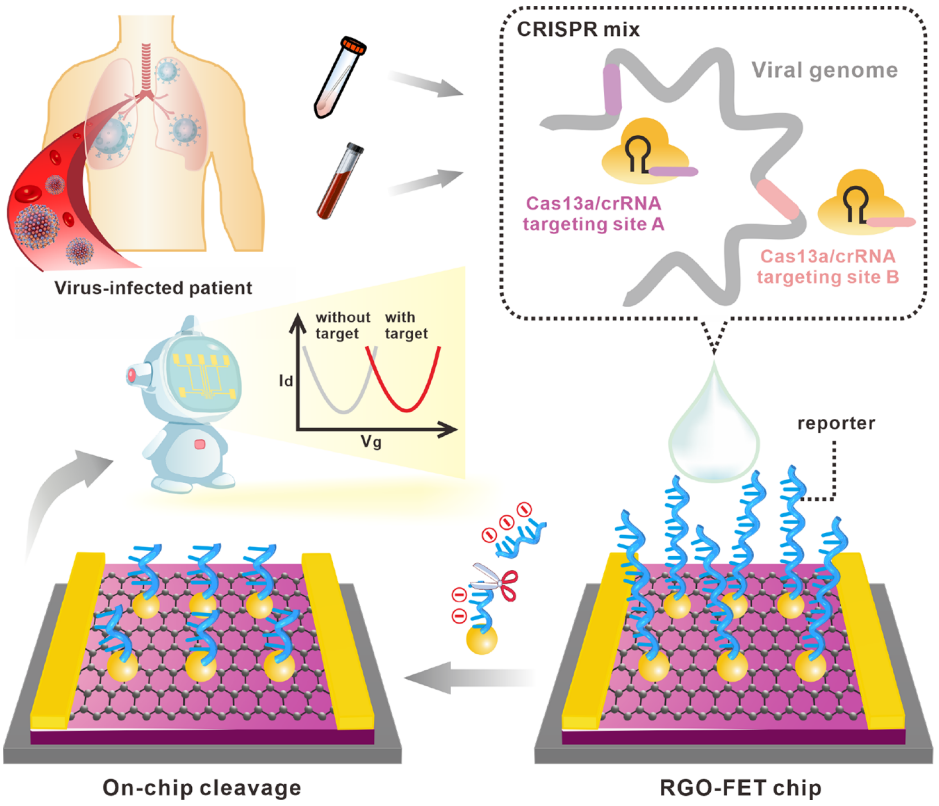

Figure 1. Principle scheme of the tandem Cas13a/crRNA-mediated CRISPR-FET biosensor for accelerated and unamplified virus detection.

phore−quencher pair, thus generating fluorescent readouts for the target level.[5] Based on this characteristic, Gootenberg et al.[6] explored a Cas13a-based diagnostic termed SHERLOCK to detect the RNA of dengue and Zika viruses with attomolar sensitivity. Zhou et al.[7] used the CRISPR/Cas13 system to identify Staphylococcus aureus in food samples with an LOD of 1 CFU/mL. What is more, a wide variety of pathogens, such as P. aeruginosa,[8] African swine fever virus (ASFV),[9] bovine viral diarrhea virus (BVDV),[10] Epstein−Barr virus (EBV),[11] and so on, have been successfully detected by CRISPR/Cas13. Nevertheless, an inevitable nucleic acid amplification protocol prior to the measurements is the common downside of such paradigms mentioned above. Despite the fact that CRISPR-based approaches are field-deployable just with a visual flow strip or portable fluorescent reader, they cannot keep up with the need for extraordinary sensitivity on their own and are frequently accompanied by tag labeling and initial pre-amplification procedures.

With the escalating demand for molecular surveillance, CRISPR technology and biosensors are mutually reinforcing with an ingenious combination, further revolutionizing nucleic acid testing.[12,13] The Cas endonuclease ability can be fully exerted through various signal transductions other than fluorescence, such as electrochemical, optical, and so on. In parallel, CRISPR/Cas paves new avenues for future applications of biosensors by serving as a programmable biomolecular element, which can sense target and spontaneously drive a particular response. Zhou et al.[14] introduced CRISPR/Cas13a into an electrochemiluminescent biosensor for highly sensitive detection of mi-RNA17 from tumor cells, wherein Cas13 activated by target miRNA could cleave a well-designed pre-primer and trigger the downstream luminescence reaction. Another research[15] constructed a Cas13-assisted electrochemical biosensor that combined catalytic hairpin assembly-mediated cascade signal enhancement to detect miRNA-21, achieving femtomolar level determination. Moreover, a CRISPR assay presented on a microfluidic biosensor was proposed for measuring the brain tumor marker miRNA-19b.[16] However, these implementations based on electrochemical or optical transduction typically require complex device design, multistep reactions, or appropriate indicative molecules to convert cleavage behavior into measurable signals, not readily entering mainstream use.

Among the numerous biosensors available today, FETs are expected to provide further opportunities for the detection of biomolecules, owing to the dominance of high speed, low power, and outstanding compatibility with integrated circuits.[17] The past few years have witnessed the ubiquitous application of graphene-based FET (G-FET) biosensors in diagnosis of various diseases, particularly viral infections such as HIV,[18] HPV,[19] EboV,[20] avian influenza virus,[21] and more, which might profit from graphene's exceedingly thin sensing layer, high carrier mobility, and good biocompatibility.[17] As such, it is anticipated that G-FET could be a desirable platform for ameliorating and enhancing the power of CRISPR-mediated diagnostics. In our previous work,[22] we have reported a morpholino-modified G-FET biosensor for rapid direct testing of SARS-CoV-2 in real time. Unfortunately, the sensitivity of this designed assay is lower than that of RT-PCR, while the method is capable of detecting viral load in clinical samples. We speculate that the integration of the CRISPR system could be an effective strategy for improving the sensitivity of G-FET sensors because the crRNA-directed cleavage is robust even at abysmally low levels of activated Cas13 protein with remarkable turnovers of at least 10^4 per target RNA bonding.[23] By coupling CRISPR and G-FET, for

https://doi.org/10.1021/acssensors.2c01200
ACS Sens. 2022, 7, 2680−2690

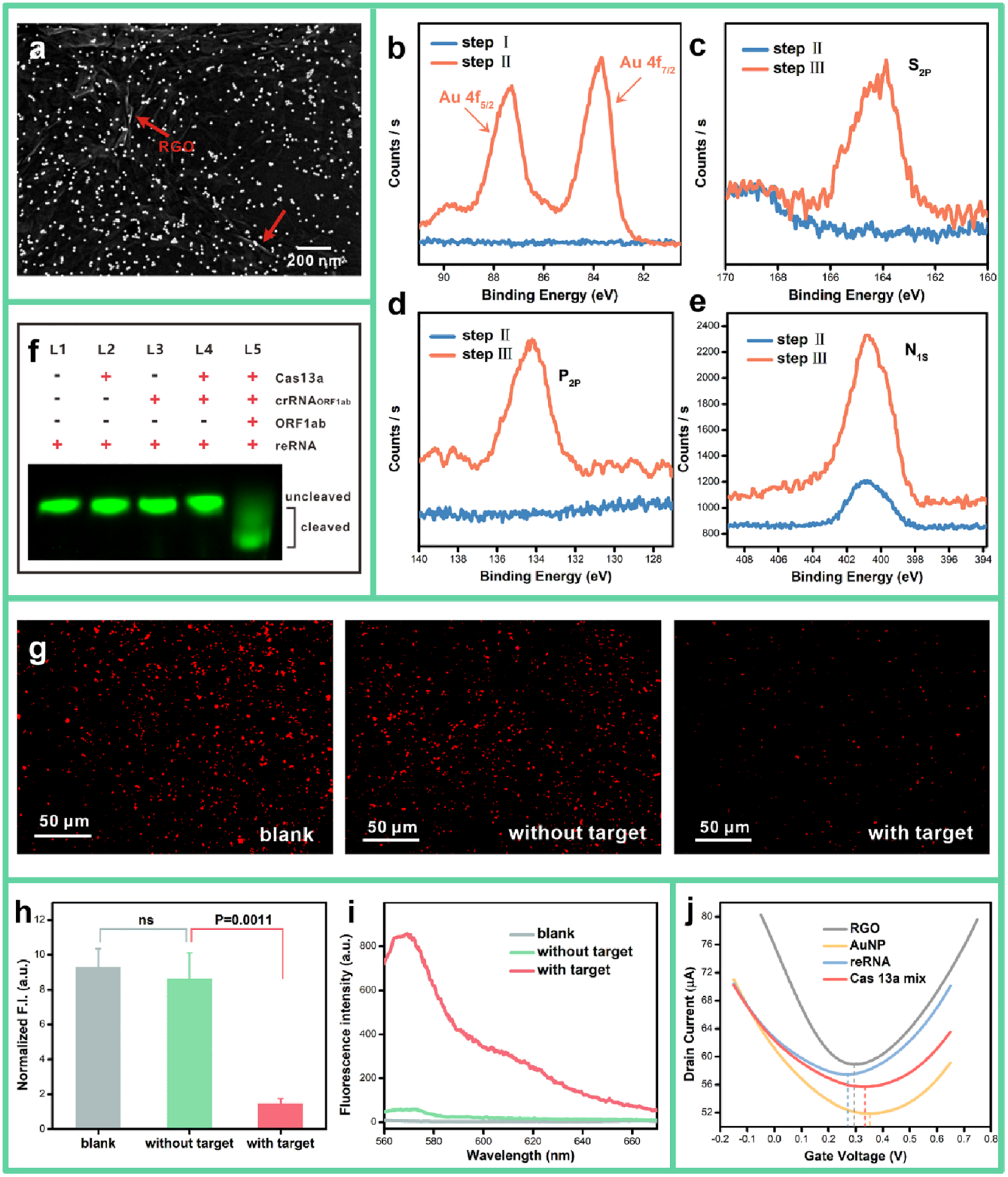

Figure 2. Characterization and feasibility of a CRISPR-FET biosensor. (a) SEM image showing deposited AuNPs on the RGO surface. Scale bar, 200 nm. (b–e) XPS spectra of Au, S, P, and N elements, respectively. (f) Electrophoretic analysis of the feasibility of the CRISPR/Cas13a reaction. "+" indicates presence and "-" indicates absence. (g) Fluorescence microscopy images of immobilized cy3-reRNA upon incubation of PBS (left), CRISPR mixture without the target (center), and complete CRISPR mixture (right). Scale bars, 50 μm. The intensities were quantified using ImageJ software (h). (i) Free Cy3 fluorescence signal in the reaction liquid recovered from the chip. (j) Stepwise I_d–V_g curves for the CRISPR-FET biosensor in the process of AuNP deposition, reRNA modification, and Cas13 cleavage action.

example, Hajian et al.[24] explored a CRISPR-Chip, which utilized the deactivated Cas9-guide RNA complexes as probes and immobilized them on the surface of graphene for DNA detection. Nevertheless, the Cas protein in this methodology

https://doi.org/10.1021/acssensors.2c01200
ACS Sens. 2022, 7, 2680–2690

was only used for precise gene recognition, and its key role as a target-triggered nuclease was neglected. More importantly, to the best of our knowledge, there are currently no reported studies aimed at the establishment of Cas13-based G-FET biosensors and their viral detection applications.

Herein, we display the unique fusion of a reduced graphene oxide (RGO)-based FET biosensor and a tandem CRISPR/Cas13a system to create a "one-for-all" check station for the direct detection of viral RNA. As shown in Figure 1, Cas13a is first integrated with crRNA whose spacer sequence is complementary to the specific site of the viral genome (site A or site B) to form a ribonucleoprotein (RNP) duplex, after which the cleavage ability of Cas13a gets activated as the RNP binds to the corresponding target. On the other hand, an AuNP-decorated RGO-FET chip is fabricated, and the thiolated reRNAs are anchored on the AuNP surface to obtain a polyvalent spherical RNA reporter, exhibiting enhanced stability and good nuclease resistance compared to the traditional ssRNA reporter used in fluorescence-based CRISPR/Cas13a diagnostics.[25] When the functionalized chip is incubated with the CRISPR mixture, the immobilized reRNAs are cleaved, inducing a p-doping with a positive shift of the Dirac point, the displacement of which reflects the target level. Through the on-chip CRISPR reaction, the FET sensor can be used to measure large-sized analytes exceeding Debye lengths, for example, the full viral genome, by sensing the target-induced cleavage of immobilized reRNA within the Debye length, offering a new potential pathway to evade the long-standing bottleneck of the Debye screening limit. What is more, thanks to the programmability of CRISPR, this platform was successfully used for the detection of CoV and HCV RNA, holding the expectation to be a multipotent scalable toolbox for FET-based diagnostics, something that cannot be done using routine receptor-modified FETs, which are restricted to single-plex assays. In addition to excellent sensitivity and single-base specificity, this assay also enjoys a decent anti-interference property in the detection of spiked target RNA. Importantly, the concomitant use of two RNPs specific to CoV ORF1ab and N genes in the same CRISPR reaction gains an impressive sensitivity, owing to the activation of double Cas13a elicited by per viral RNA. Moreover, from a clinical feasibility dimension, we demonstrate that the developed sensor mediated by dual-RNP in tandem can completely distinguish HCV positive people from negative ones, circumventing nucleic acid amplification and its attendant risk of cross-contamination.

RESULTS AND DISCUSSION

Construction and Verification of a CRISPR-FET Biosensor. The fabrication of the CRISPR-FET chip, as illustrated in Figure S1, comprises a three-step workflow of RGO deposition (step I), AuNP decoration (step II), and reRNA immobilization (step III). To ensure that the device was successfully established, multiple characterizations were executed. Figure 2a,b presents scanning electron microscopy (SEM) and X-ray photoelectron spectroscopy (XPS) results, respectively, which manifests that high density AuNPs around 10 nm diameter were ideally formed on the RGO surface. The large surface area of AuNPs not only increases the amount of immobilized reRNA but also creates a greater space for Cas13a to perform cleavage activity compared with the direct connection of reRNAs to the channel surface, reducing the probable steric hindrance of on-chip CRISPR reaction. Then, the appearance of the S_{2P} peak (163.9 eV) and the P_{2P} peak (134.2 eV) and a marked intensification of the N_{1S} peak (400.8) in the XPS spectrum after step III prove the successful assembly of reRNA through Au−S bonds (Figure 2c−e). A much weaker N_{1s} peak (blue line) observed in step II was from the possible presence of N element in hydrazine.

In view of the two significant factors affecting the initiation of the CRISPR reaction, which are the optimum length range of the crRNA spacer region and a strong cleavage preference of LwaCas13a for U-rich sequences,[8] we elaborately designed crRNAs and reRNAs as shown in Table S1. For proof-of-concept, the synthetic CoV ORF1ab gene was used as a validation model for the follow-up experiments, and the 15 nt reRNA was used. First, the fluorescence assay was carried out to verify that reRNA could be degraded exclusively in the presence of target as anticipated. It can be seen from Figure S2 that the fluorescence strengthened in intensity with increasing target abundance, ascribed to the gradually increasing destruction of FAM-BHQ1-labeled reRNAs, while the FAM signal disappeared in the absence of ORF1ab RNA. Also, as shown in Figure 2f, similar results were obtained by further PAGE electrophoresis where the faster migrating bands representing cleavage products can only be observed upon the addition of target (lane 5).

Motivated by these results, we wondered whether the cleavage was also allowed for immobilized reRNA on the fabricated RGO-FET chip. For this experiment, we used cy3-labeled thiolated reRNA to modify the CRISPR-FET chips and then introduced PBS, a CRISPR mixture without target, and a complete mixture system to the devices. Following incubation, as indicated in Figure 2g, the control chips (without target; center panel) showed a similar obvious red fluorescence to the blank condition (left panel), whereas a drastically weaker red fluorescence was imaged for experimental groups (with target; right panel). To make a more intuitive comparison, the fluorescence intensity of three groups of chips was quantified using ImageJ[26] (V. 1.53a) (Figure 2h). On the other hand, reaction solutions were recovered from the chip surface after 30 min of incubation and underwent fluorescence measurement using a fluorescence spectrophotometer with cy3 excitation/emission wavelengths at 550/570 nm (Figure 2i). As expected, a significant fluorescent readout was detected in the experimental group whose recovery solution contained the free cy3 fluorescent moieties released from the AuNPs due to the target-induced cleavage effect. Combining the fluorescence assay results in solid and liquid phases, it can be demonstrated that the CRISPR system used in this work was capable of hydrolyzing the immobilized reRNAs effectively. Furthermore, the construction and feasibility of the CRISPR-FET chip were also supported by electrical characterization with step-by-step I_d-V_g transfer curves (Figure 2j). In alignment with previous reports,[27] the Dirac point traveled to the positive direction due to p-doping after AuNP deposition (yellow line). While a plethora of negative charges carried by reRNA led to n-doping (blue line). Then, the Dirac point showed a positive shift again (red line) because the activated Cas13a destructed the reRNAs.

Optimization of the Experimental Conditions. To prepare for a satisfactory detection performance, several critical conditions were optimized. We first evaluated the effect of different reRNA lengths (15, 25, 35, and 45 nt) on the cleavage activity of Cas13a. As shown in Figure S3a, the greatest variation of the gate voltage for Dirac point (ΔV_{CNP}) was

https://doi.org/10.1021/acssensors.2c01200
ACS Sens. 2022, 7, 2680−2690

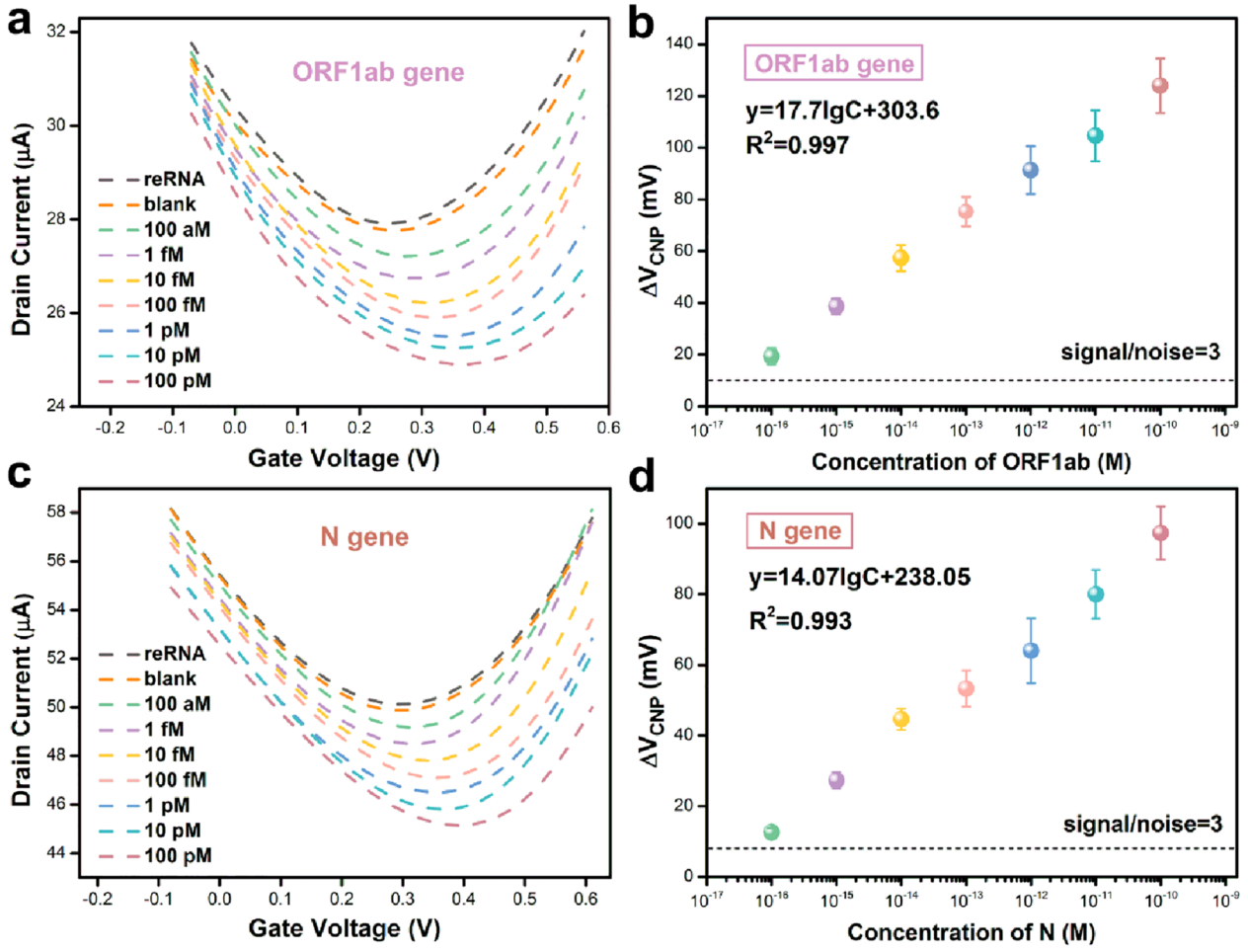

Figure 3. Direct detection of synthetic sequences using the CRISPR-FET assay. (a,c) Transfer curves with varying concentrations of the CoV ORF1ab gene and N gene. (b,d) Calibration curves between ΔV_{CNP} response versus different contents of ORF1ab and N gene. The dashed lines symbolize 3-fold noise levels, which are 10 and 8 mV, respectively. Values represent mean ± SD (n = 3).

obtained at a length of 25 nt reRNA. However, the FET signal decreased when the reRNA was too short or too long. The 15 nt reRNA brought about only a small reduction in negative charge under the digestion event. As for a too long reRNA, although a greater charge change was generated per reRNA cleavage on the channel surface, a possible secondary structure declined the overall digestion efficiency. Moreover, it would take more time to degrade a longer reRNA.[25] Therefore, the 25 nt reRNA was selected to functionalize the CRISPR-FET sensor. Additionally, we optimized the reRNA concentration and incubation time (Figure S3b,c). Because the high coverage of reRNA caused steric hindrance, inhibiting the accessibility of Cas13a to the immobilized reRNA, the optimal concentration was eventually found to be 10 μM. Furthermore, different incubation times did not evoke a considerable variation in the sensing signal. Also, it is worth noting that the ΔV_{CNP} decreased slightly at 2 h, which may be related to non-specific adsorption in the prolonged incubation time, thereby affecting the charge doping. Thus, 0.5 h was selected for subsequent applications.

Sensitivity. To investigate the sensitivity of the CRISPR-FET biosensor for ORF1ab RNA detection, CRISPR/Cas13a mixtures, inclusive of Cas13a, $crRNA_{ORF1ab}$, cleavage buffer, RNase inhibitor, and diverse concentrations of the ORF1ab gene from 100 aM to 100 pM, were introduced to the devices successively under optimal conditions. As illustrated in Figure 3a, the Dirac point presented a progressive positive shift with increasing amounts of target RNA. The average signal values corresponding to various contents ranging from 100 aM to 100 pM were 19, 39, 57, 75, 91, 105, and 124 mV. Moreover, the calibration curve in Figure 3b exhibited good linearity (R^2 = 0.997) between the logarithms of the ORF1ab concentration and the response signal, with a regression equation of ΔV_{CNP} = 17.7 lg$C$ + 303.6. Grounded on a signal-to-noise ratio of 3, the LOD was as low as 25 aM, equivalent to the copy number concentration of 1.5 × 10^4 copies/mL. Notably, the sensitivity improved by 2 orders of magnitude compared with a direct Cas13-based RNA detection (10^6 copies/mL)[28] and achieved a 100-fold increase over the work of Cui et al., in which RNA was gauged by a Cas13a-powered electrochemical biosensor with an LOD of 2.6 fM.[15] This impressive sensitivity elucidates that the proposed CRISPR-FET assay extends the boundaries of detection ability for CRISPR technology. We attribute such excellent performance to RGO with high conductivity, and Cas13a serves as a signal amplifier in cleavage duration with a high turnover. Additionally, we attempt to determine the ORF1ab gene in real time under the gate voltage of 0.2 V and drain voltage of 0.1 V. As shown in Figure S4, upon injection of the CRISPR mixture with a certain concentration of target, the drain current declined steeply in a matter of minutes. Furthermore, here, good sensitivity with permission for 1 fM ORF1ab to be detected was also realized in real-time

https://doi.org/10.1021/acssensors.2c01200
ACS Sens. 2022, 7, 2680−2690

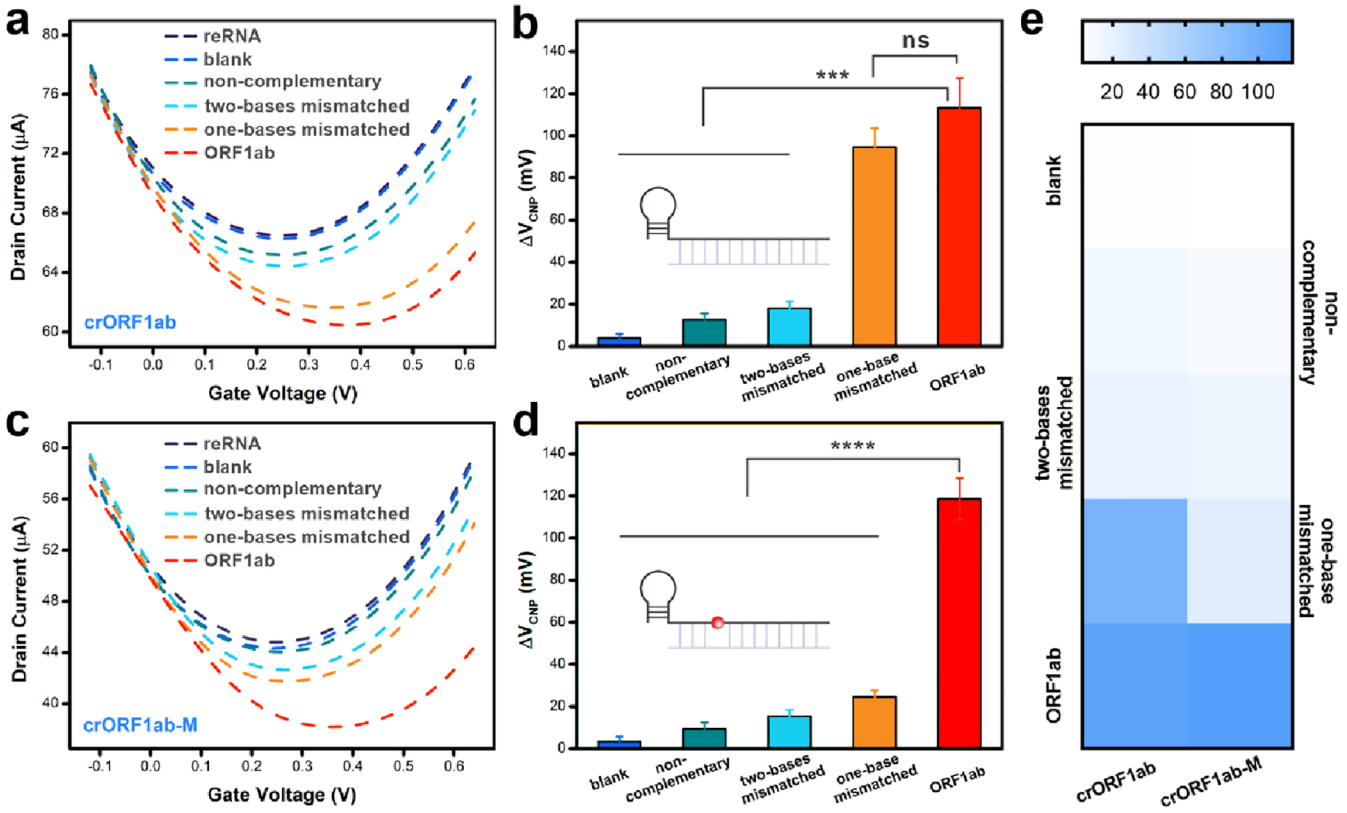

Figure 4. Specificity toward a single base for the CRISPR-FET sensor can be achieved by introducing a mismatch into the crRNA spacer. (a,b) Sensing signals for non-specific sequences and ORF1ab RNA, with a complementary crRNA (crORF1ab). (c,d) Sensing signals for non-specific sequences and ORF1ab RNA, with a crRNA introducing an intentional mismatch (crORF1ab-M). (e) Heat map depicting the detection results applying crORF1ab and crORF1ab-M across non-specific RNA and target RNA.

measurement. What is more, we further examined the CoV N gene by leveraging a corresponding crRNA with a complementary spacer sequence. Figure 3c,d clearly demonstrates that the developed method also successfully detected the N gene with a satisfactory LOD of 44 aM (2.65×10^4 copies/mL), and the linear equation is expressed as $\Delta V_{CNP} = 14.07 \lg C + 238.05$ with R^2 equal to 0.993. These results reveal an exciting highlight that the programmability of crRNA renders our biosensor a "one-for-all" platform, which virtually allows the detection of any RNA without having to fabricate a new device, just by expediently using a target-specific crRNA in the CRISPR reaction.

Specificity. We then studied the discrimination ability of the CRISPR-FET sensor between the target RNA and other contaminant RNAs. For this experimental setting, ORF1ab was maintained as an assessment model, and four CRISPR mixtures containing several 1 nM non-complementary RNA, two-base mismatched RNA, one-base mismatched RNA, and 100 pM ORF1ab RNA were successively incubated on the sensor chip. Apparently, as shown in Figure 4a,b, there was only negligible movement of the Dirac point upon interaction with blank, non-complementary RNA, and two-base mismatched RNA, with the ΔV_{CNP} value of 4, 13, and 18 mV, respectively. Whereas, in conformity with literature reports regarding the single mismatch tolerance of Cas13a/crRNA,[6,14,29] a remarkable response up to 94 mV was observed after exposure with one-base mismatched RNA, which had no significant difference with the signal intensity conferred by the target RNA. To obviate this phenomenon, a synthetic mismatch was artificially introduced into the crRNA spacer region (Figure 4c,d). Satisfyingly, the spurious sensing signal produced by one-base mismatched RNA dramatically diminished compared to that in the case of applying a perfectly complementary crRNA (crORF1ab). Therefore, as highlighted in the heat map (Figure 4e), the crRNA with an intentional mismatch (crORF1ab-M) can contribute a higher resolution for CoV RNA detection, even enabling single-base specificity.

Anti-interference Capability. In order to guarantee practical relevance, we assessed the anti-interference capability of the sensor within biological contexts. Briefly, negative throat swabs were spiked with ORF1ab or N sequences. The obtained contrived samples harboring target RNA at different concentrations were tested using the developed method, following the same protocol adopted in reference RNA solutions. As we can see, the signal output was slightly less pronounced but still striking enough in detection of both spiked ORF1ab and N gene samples. Meanwhile, a relatively low background was also achieved even in the complex matrix environment (Figure 5a–c). Consequently, the obtained sensor possesses outstanding capacity to resist interference, displaying a promising application in clinical settings.

Tandem Cas13a-crRNA-Mediated Virus Detection. Considering that a credible clinical application is highly demanding in terms of sensitivity, attempts to further increase detection sensitivity had been made prior to analyzing patient samples. Herein, we exploited a dual Cas13a-crRNA strategy by combining crRNAs in tandem which targeted the ORF1ab and N gene, respectively, to form two different Cas13a-crRNA complexes, namely, RNP. For validation, we tested a positive control material for CoV containing the whole viral genome via

https://doi.org/10.1021/acssensors.2c01200
ACS Sens. 2022, 7, 2680−2690

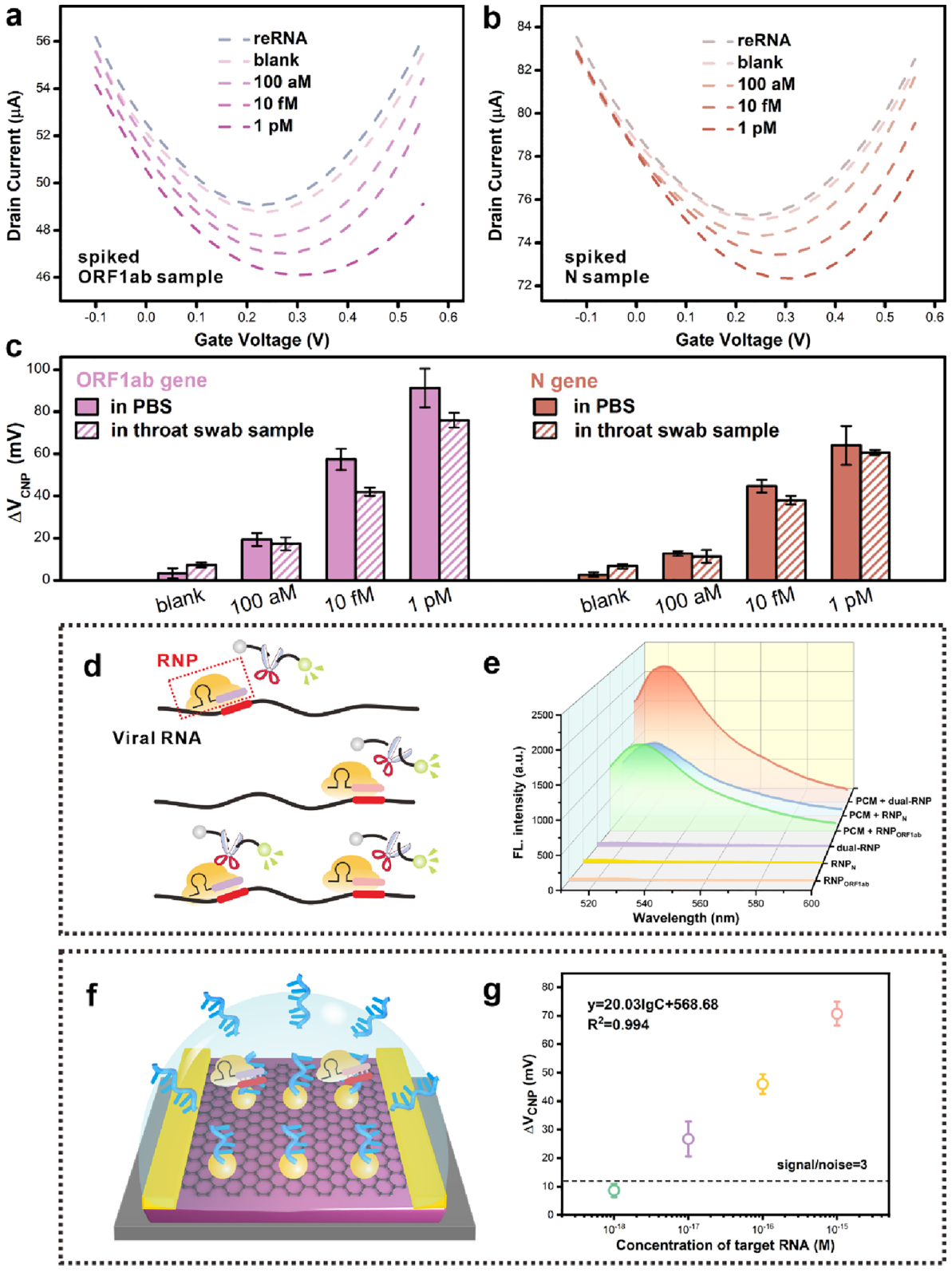

Figure 5. Excellent anti-interference capability and dual-RNP-assisted signal amplification. (a) I_d−V_g curves upon detection of the ORF1ab gene spiked in throat swab samples. (b) I_d−V_g curves upon detection of N gene spiked in throat swab samples. (c) Comparison of detection results for ORF1ab and N genes in PBS and throat swab by the developed sensor. (d) Schematic of the Cas13a (yellow)-crRNAORF1ab (purple) RNP complex and Cas13a (yellow)-crRNAN (pink) RNP complex individually or simultaneously binding to the CoV genome, leading to the triggering of the Cas13a cleavage event. (e) Fluorescence testing of a positive control material for CoV containing the whole viral genome with the CRISPR/Cas13a cleavage assay with single RNP and dual-RNP, respectively. (f) Schematic of the on-chip cleavage reaction driven by dual-RNP, which can amplify the FET response. (g) Calibration curve at diverse concentrations of Mix 2 under a dual-RNP strategy. The dashed line symbolizes a 3-fold noise level (12 mV).

https://doi.org/10.1021/acssensors.2c01200
ACS Sens. 2022, 7, 2680−2690

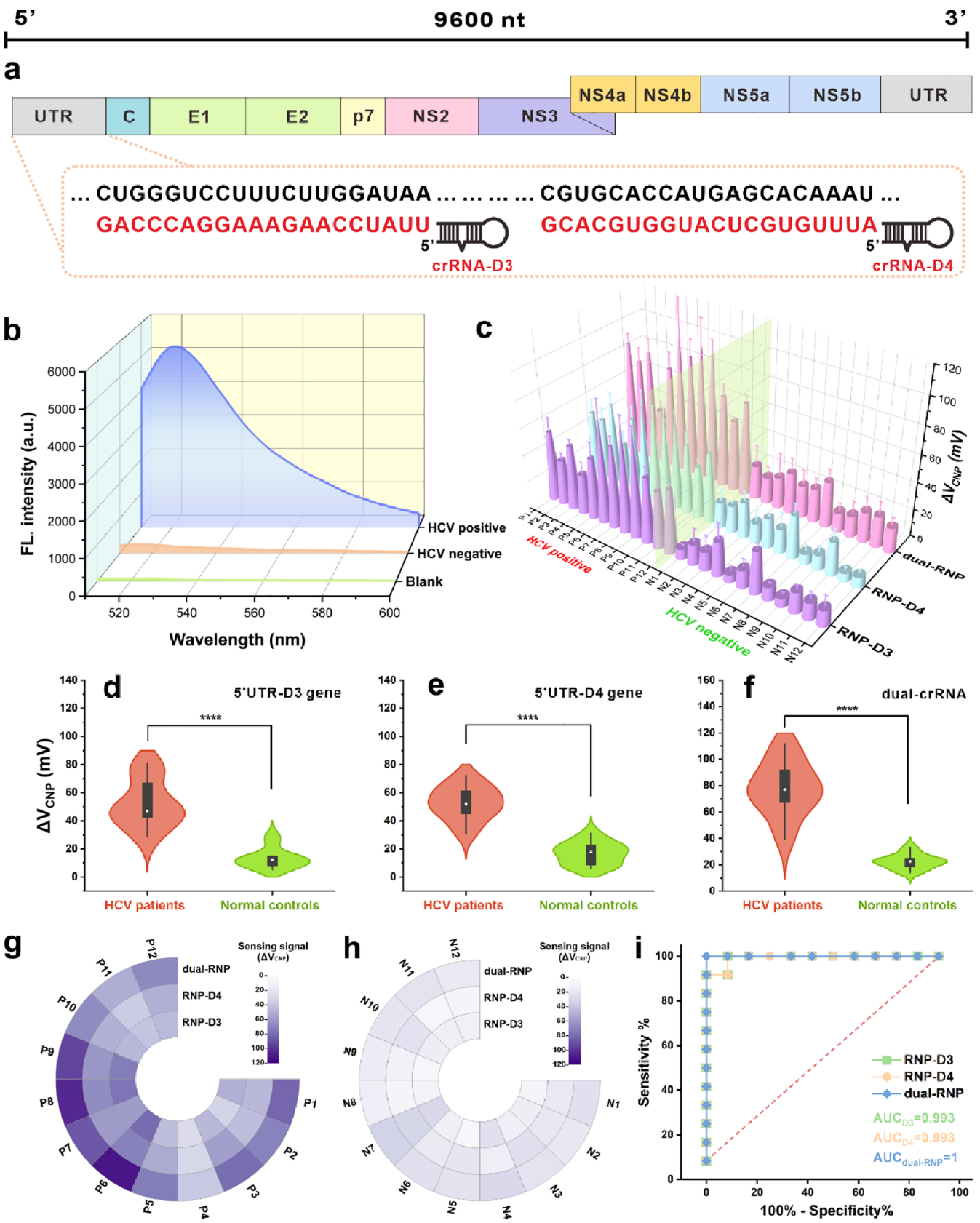

Figure 6. Favorable diagnostic performance of the CRISPR-FET sensor for clinical samples. (a) HCV genome map and genomic coordinates of detected sequences. (b) Fluorescence verification of an HCV-positive specimen with dual-RNP. (c) ΔV_{CNP} values of 24 clinical samples under the conditions of single RNP for D3, single RNP for D4, and dual RNP. (d) Significant difference of 5′UTR D3 in response to HCV patients and healthy controls. (e) Significant difference of 5′UTR D4 in response to HCV patients and healthy controls. (f) Significant difference in response to HCV patients and healthy controls with dual-RNP-targeted testing. (g,h) Heat maps showing the intensity of the sensing signal across 12 HCV positive and 12 negative samples with single- and dual-RNP testing. (i) ROC analysis of the CRISPR-FET sensor in response to clinical samples.

https://doi.org/10.1021/acssensors.2c01200
ACS Sens. 2022, 7, 2680−2690

the traditional CRISPR assay, with 100 nM single RNP_{ORF1ab}, 100 nM single RNP_N, and 100 nM dual RNP (50 nM each of RNP), respectively. In this strategy, theoretically, an individual CoV RNA could activate double Cas13a due to simultaneous identification of two sites, leading to more cleavages of FAM-BHQ1 reRNAs, as shown in Figure 5d. Consistent with literature studies,[28,30] we found that the fluorescence strength was due to substantial augment in the dual-RNP reaction (Figure 5e). These results suggest that RNPs in combination can effectively amplify signals. At the same time, it also clarifies that the method is applicable for the detection of large-sized full-length viral RNA. To survey how RNP combinations affect the detection limit, we mixed ORF1ab and N RNA solutions in a 1:1 M ratio ("Mix 2") to get close to the real detection situation, where the full viral genome was tested. Then, a series of dilutions of Mix 2 were measured using the CRISPR-FET sensor with the dual-RNP strategy (Figure 5f). As described in Figure 5g, an LOD as low as 1.56 aM (940 copies/mL) was obtained, which is about 20-fold lower than that of the single RNP condition (Figure 3). This breakthrough makes the sensitivity of the developed sensor commensurate with that of RT-PCR,[31] concurrently averting the nucleic acid amplification. What is more, the synergy of two crRNAs targeting different regions of the viral genome can reduce the likelihood of missing inspection resulting from viral mutations or viral RNA's partial degradation.

Analysis of Clinical HCV Infections with the CRISPR-FET Biosensor. The ultimate goal for a reliable biosensor is to be amenable to clinical diagnosis, whereupon we injected impetus to the practical application. To further corroborate the ability of the CRISPR-FET as a "one-for-all" platform, that is, generic, versatile, and pleiotropic, this devised sensor was also employed in the detection of HCV RNA. HCV infection is a menacing global health problem, with a huge burden of more than 71 million people being affected worldwide according to a recent modeling study.[32] In addition to the well-known severe, life-long liver complications, such as chronic hepatitis and cirrhosis, which can finally end with hepatocellular carcinoma, HCV has also been blamed for numerous extra hepatic manifestations including heart diseases, rheumatologic disorders, diabetes mellitus, and so forth.[33] With the advent of oral direct-acting antivirals (DAAs), a new hepatitis C treatment with a short duration and low toxicity has emerged. Based on those efforts, the WHO has set an ambitious objective of eliminating HCV infection by 2030.[34] However, the under-diagnosis remains a chief obstacle in the progress toward global eradication. Therefore, a special spotlight is deserved for the exploration of more sensitive, affordable, and facile screening technologies for HCV. Grounded on the efficacious and marvelous performance in CoV RNA testing, it is conceivable that the developed CRISPR-FET is competent for fulfilling its transformative role in ascertaining HCV RNA. Analogous to CoV, HCV is a single-stranded, positive-sense RNA virus whose genome comprises approximately 9600 nucleotides, containing a long open-reading frame region in the middle and 5', 3′ untranslated regions (UTRs) at both ends. Thereof, the 5′UTR embracing four major structural domains (domains I–IV) is the most conserved region with more than 90% of the sequences identical in different HCV genotypes.[35] We consequently selected the domains III (D3) and IV (D4) of the 5′UTR as recognition sequences and designed the corresponding crRNAs (Figure 6a). Following this lead, the HCV-induced cleavage was first proved by a fluorescence measurement with dual-crRNA guiding which targets D3 and D4, respectively (Figure 6b). Thereafter, four series of 10-fold dilutions of an HCV-positive serum specimen were tested using the CRISPR-FET sensor. Since the target level is reflected by the target-induced cleavage sensing, for the developed method, we do not need to consider whether the determinant is beneath the Debye length boundary, even in the detection of large viral RNA in clinical samples. As shown in Figure S5, there is a great linear correlation between the above-noise response and the dilution factor (R^2 = 0.9897), suggesting that this assay has the potential to accurately quantify clinical samples. Encouraged by the results, we then performed the CRISPR-FET sensor to detect 24 clinical serum RNA extracts from 12 HCV-positive patients and 12 non-HCV normal people, which had been confirmed by RT-PCR, and the Ct values are displayed in Table S2. Figure 6c depicts the sensing signals of 24 samples under the conditions of single RNP for D3, single RNP for D4, and dual RNP. Figure 6d–f reflect significantly distinguishable response levels in patients versus controls with p values <0.0001. What is more, the heat maps (Figure 6g,h) give an intuitive and comprehensive comparison. It can be explicitly seen that dual RNP gave rise to more phenomenal ΔV_{CNP} values than each individual RNP. Intriguingly, a missed detection appeared in positive sample #4 on separate measurements for the D3 or D4 gene. However, dual RNP-targeted testing made it detectable. We conjectured that this was probably because the target RNA partially degraded during storage. Hence, it is believed that the utilization of dual-RNP plays an imperative part in obviating false-negative judgments for the CRISPR-FET sensor. To gain an ample insight into diagnostic performance, the receiver operating characteristic curve (ROC) was implemented (Figure 6i). Unsurprisingly, superior accuracy (AUC = 1) was achieved in the dual RNP-based CRISPR-FET assay, which perfectly distinguished HCV infection patients from healthy ones.

CONCLUSIONS

In this work, we have made a remarkable conceptual advance in the FET field, that is, the tandem Cas13a-crRNA-mediated CRISPR-FET biosensor, a pluripotent platform, has been developed for unamplified diagnosis of CoV, HCV, and even other arbitrary viruses in the future. Under optimized conditions, this sensor could provide quite a low detection limit of 25 aM for the CoV ORF1ab gene and 44 aM for the CoV N gene. Moreover, a single-base resolution is realized by introducing an intentional mismatch into crRNA. Strikingly, the good anti-interference capability lays a springboard toward practical application. A noteworthy leap forward is that the dual-RNP strategy of deploying crRNAs for different gene loci in tandem increases the sensitivity of the sensor by about 20 times with the LOD of 1.56 aM (940 copies/mL), which can rival the RT-PCR.[33] Even more, a complete discrimination, bypassing PCR, of HCV-positive and -negative volunteers was achieved, promoting the alignment of this prototype methodology with clinical acceptability. Such superior analytical performances, compared to other FET sensors (Table S3), represent an important step forward toward a desirable virus diagnosis technology in the FET field. This study has integrated, for the first time, the CRISPR/Cas13 system and the FET sensor, taking full advantage of the self-amplifying effect, target-induced ribonuclease activity of Cas13a, and the high sensitivity and fast response of FET. As one of the few

https://doi.org/10.1021/acssensors.2c01200
ACS Sens. 2022, 7, 2680−2690

molecular diagnostic techniques removing the amplification step, this approach lowers the cross-contamination risk for both intra- and inter-batches of samples, especially during the universal nucleic acid testing in medium−high risk areas. This sensing platform unlocks the great potential of large-scale screening and field-deployable identification. Furthermore, by reasonably programming the crRNA spacer, the developed CRISPR-FET sensor can evolve into a versatile "one-for-all" check station, which opens more exciting possibilities for conquering the current pandemic and future infectious disease outbreaks. Collectively, we envision that this ground-breaking sensing platform can be a significant drive to deliver FET solutions to healthcare.

EXPERIMENTAL METHODS

Reagents and Materials. Graphene oxide (GO) powders were offered by Alfa Aesar Co. Ltd. Hydrazine (98%) and $HAuCl_4 \cdot 3H_2O$ were supplied by Aladdin Co. Ltd. 6-Mercapto-1-hexanol (MCH), tris(2-carboxyethyl) phosphine hydrochloride (TCEP), and RNase-ZAP were bought from Sigma-Aldrich. LwaCas13a (Cas13a from *Leptotrichia wadei*) (E381) and murine RNase inhibitor (E125) were provided by Novoprotein Scientific Inc. Molecular biology grade ultrapure water was purchased from GENOM Inc. All selected and designed RNA sequences as listed in Table S1 were synthesized by Sangon Biotech. Clinical serum specimens were collected from the Affiliated Hospital of Hubei University of Chinese Medicine, with the approval of the ethics committee.

Fabrication of the CRISPR-FET Biosensor. The preparation of RGO and the production of the RGO-based FET chip were carried out according to our previous reports.[22,36] By immersing the RGO-FET chip in a 10 μL of 10 mM $HAuCl_4$ solution, the AuNPs could be deposited spontaneously on the RGO surface via direct redox reactions between metal ions and RGO. Subsequently, the resulting AuNP-decorated RGO-FET chip was incubated with 10 μL of TCEP-pretreated thiolated reRNA overnight. After washing and drying, the reRNA-modified device experienced a blocking process with 10 μL of 2 mM MCH. Then, the final CRISPR-FET biosensor was obtained and could be used for follow-up experiments.

Fluorescent Cas13a Cleavage Assay. 1 μL of Cas13a and 5 μL of 100 nM crRNA were incubated for 10 min at room temperature to preassemble the RNP complex, followed by the addition of 5 μL of target RNA, 1 μL of FAM-BHQ1-labeled reRNA (10 μM), 1 μL of murine RNase inhibitor, and 2 μL of cleavage buffer to obtain 15 μL of reaction mixture. For assays involving the dual-RNP strategy, the Cas13a-crRNA$_{ORF1ab}$ and Cas13a-crRNA$_N$ complexes were separately preassembled by incubating for 10 min. Then, two RNPs at half volume were mixed with the other reaction components to maintain the total RNP concentration constant. After 30 min of incubation at 37 °C, the mixture was measured using a fluorescence spectrophotometer with the FAM channel (λex/λem at 490/520 nm).

CRISPR-FET Assay for Viral RNA Detection. Similar to the preprocessing step for the fluorescent Cas13a assay, the CRISPR reaction mixture was prepared, but no reRNA was added. The RNaseZap-treated CRISPR-FET chip was then exposed to the mixture for 30 min at 37 °C, followed by thorough elution to flush out the free reRNA fragment cleaved from the secured reRNA mounted on the AuNP surface. For electrical measurement, the I_d−V_g transfer curves pre- and post-incubation were recorded using a semiconductor analyzer and a probe station at 0.1 V bias and a liquid gate with 0.01 × PBS. A silver wire was used as the gate material for the liquid gate.

ASSOCIATED CONTENT

Supporting Information

The Supporting Information is available free of charge at https://pubs.acs.org/doi/10.1021/acssensors.2c01200.

Additional data including the RNA sequences used in this work, device fabrication schematic, fluorescence verification results of CRISPR/Cas13a cleavage, condition optimization results, real-time measurements of ORF1ab, RT-PCR results of clinical samples, and comparison of our sensor with other FET-based virus detection methods (PDF)

AUTHOR INFORMATION

Corresponding Authors

Youyun Zhao − *Hubei Provincial Hospital of Traditional Chinese Medicine, Wuhan 430061, China*; Phone: +86-27-68890259; Email: zhaoyy206@163.com; Fax: +86-27-68890259

Zhi-Yong Zhang − *Hunan Institute of Advanced Sensing and Information Technology, Xiangtan University, Hunan 411105, P. R. China*; orcid.org/0000-0003-1622-3447; Email: zyzhang@pku.edu.cn

Guo-Jun Zhang − *School of Laboratory Medicine, Hubei University of Chinese Medicine, Wuhan 430065, P.R. China*; orcid.org/0000-0001-9096-9226; Email: zhanggj@hbtcm.edu.cn

Authors

Jiahao Li − *School of Laboratory Medicine, Hubei University of Chinese Medicine, Wuhan 430065, P.R. China*; orcid.org/0000-0002-4107-7720

Lina Tang − *School of Laboratory Medicine, Hubei University of Chinese Medicine, Wuhan 430065, P.R. China*

Tingxian Li − *School of Laboratory Medicine, Hubei University of Chinese Medicine, Wuhan 430065, P.R. China*

Kun Li − *School of Laboratory Medicine, Hubei University of Chinese Medicine, Wuhan 430065, P.R. China*

Yulin Zhang − *School of Laboratory Medicine, Hubei University of Chinese Medicine, Wuhan 430065, P.R. China*

Wei Ni − *Hubei Provincial Hospital of Traditional Chinese Medicine, Wuhan 430061, China*

Meng-Meng Xiao − *Hunan Institute of Advanced Sensing and Information Technology, Xiangtan University, Hunan 411105, P. R. China*

Complete contact information is available at: https://pubs.acs.org/10.1021/acssensors.2c01200

Author Contributions

J.L. and T.L. contributed equally to the work. J.L. performed the experiments and wrote the original draft; L.T. performed sample treatment and clinical analysis; T.L., K.L., W.N., and Y.Z. participated in this work; M.-M.X. performed chip fabrication; Y.Z. and Z.-Z.Z. were involved in supervision and writing—reviewing and editing; G.-J.Z. was in charge of supervision, project administration, writing—review and editing, and funding acquisition. All authors commented on and discussed this work.

Notes

The authors declare no competing financial interest.

ACKNOWLEDGMENTS

This work was supported by the National Natural Science Foundation of China (21974035).

REFERENCES

(1) Li, D.; Chen, H.; Gao, X.; Mei, X.; Yang, L. Development of General Methods for Detection of Virus by Engineering Fluorescent Silver Nanoclusters. *ACS Sens* **2021**, *6*, 613−627.

(2) Zhou, L.; Peng, R. X.; Zhang, R.; Li, J. M. The applications of CRISPR/Cas system in molecular detection. *J. Cell Mol. Med.* **2018**, *22*, 5807−5815.
(3) Abudayyeh, O. O.; Gootenberg, J. S.; Konermann, S.; Joung, J.; Slaymaker, I. M.; Cox, D. B.; Shmakov, S.; Makarova, K. S.; Semenova, E.; Minakhin, L.; Severinov, K.; Regev, A.; Lander, E. S.; Koonin, E. V.; Zhang, F. C2c2 is a single-component programmable RNA-guided RNA-targeting CRISPR effector. *Science* **2016**, *353*, aaf5573.
(4) Abudayyeh, O. O.; Gootenberg, J. S.; Essletzbichler, P.; Han, S.; Joung, J.; Belanto, J. J.; Verdine, V.; Cox, D.; Kellner, M. J.; Regev, A.; Lander, E. S.; Voytas, D. F.; Ting, A. Y.; Zhang, F. RNA targeting with CRISPR-Cas13. *Nature* **2017**, *550*, 280−284.
(5) Gao, D. S.; Zhu, X. D.; Lu, B. F. Development and application of sensitive, specific, and rapid CRISPR-Cas13-based diagnosis. *J. Med. Virol.* **2021**, *93*, 4198−4204.
(6) Gootenberg, J. S.; Abudayyeh, O. O.; Lee, J. W.; Essletzbichler, P.; Dy, A. J.; Joung, J.; Verdine, V.; Donghia, N.; Daringer, N. M.; Freije, C. A.; Myhrvold, C.; Bhattacharyya, R. P.; Livny, J.; Regev, A.; Koonin, E. V.; Hung, D. T.; Sabeti, P. C.; Collins, J. J.; Zhang, F. Nucleic acid detection with CRISPR-Cas13a/C2c2. *Science* **2017**, *356*, 438−442.
(7) Zhou, J.; Yin, L.; Dong, Y.; Peng, L.; Liu, G.; Man, S.; Ma, L. CRISPR-Cas13a based bacterial detection platform: Sensing pathogen Staphylococcus aureus in food samples. *Anal. Chim. Acta* **2020**, *1127*, 225−233.
(8) Gootenberg, J. S.; Abudayyeh, O. O.; Kellner, M. J.; Joung, J.; Collins, J. J.; Zhang, F. Multiplexed and portable nucleic acid detection platform with Cas13, Cas12a, and Csm6. *Science* **2018**, *360*, 439−444.
(9) Ren, M.; Mei, H.; Zhou, M.; Fu, Z. F.; Han, H.; Bi, D.; Peng, F.; Zhao, L. Development of A Super-Sensitive Diagnostic Method for African Swine Fever Using CRISPR Techniques. *Virol. Sin.* **2021**, *36*, 220−230.
(10) Yao, R.; Xu, Y.; Wang, L.; Wang, D.; Ren, L.; Ren, C.; Li, C.; Li, X.; Ni, W.; He, Y.; Hu, R.; Guo, T.; Li, Y.; Li, L.; Wang, X.; Hu, S. CRISPR-Cas13a-Based Detection for Bovine Viral Diarrhea Virus. *Front. Vet. Sci.* **2021**, *8*, 603919.
(11) Wu, Y. T.; Liu, S. X.; Wang, F.; Zeng, M. S. Room Temperature Detection of Plasma Epstein-Barr Virus DNA with CRISPR-Cas13. *Clin. Chem.* **2019**, *65*, 591−592.
(12) Aman, R.; Mahas, A.; Mahfouz, M. Nucleic Acid Detection Using CRISPR/Cas Biosensing Technologies. *ACS Synth. Biol.* **2020**, *9*, 1226−1233.
(13) Li, Y.; Li, S. Y.; Wang, J.; Liu, G. CRISPR/Cas Systems toward Next-Generation Biosensing. *Trends Biotechnol.* **2019**, *37*, 730−743.
(14) Zhou, T.; Huang, R.; Huang, M.; Shen, J.; Shan, Y.; Xing, D. CRISPR/Cas13a Powered Portable Electrochemiluminescence Chip for Ultrasensitive and Specific MiRNA Detection. *Adv. Sci.* **2020**, *7*, 1903661.
(15) Cui, Y.; Fan, S.; Yuan, Z.; Song, M.; Hu, J.; Qian, D.; Zhen, D.; Li, J.; Zhu, B. Ultrasensitive electrochemical assay for microRNA-21 based on CRISPR/Cas13a-assisted catalytic hairpin assembly. *Talanta* **2021**, *224*, 121878.
(16) Bruch, R.; Baaske, J.; Chatelle, C.; Meirich, M.; Madlener, S.; Weber, W.; Dincer, C.; Urban, G. A. CRISPR/Cas13a-Powered Electrochemical Microfluidic Biosensor for Nucleic Acid Amplification-Free miRNA Diagnostics. *Adv. Mater.* **2019**, *31*, No. e1905311.
(17) Dai, C.; Liu, Y.; Wei, D. Two-Dimensional Field-Effect Transistor Sensors: The Road toward Commercialization. *Chem. Rev.* **2022**, *122*, 10319−10392.
(18) Islam, S.; Shukla, S.; Bajpai, V. K.; Han, Y. K.; Huh, Y. S.; Kumar, A.; Ghosh, A.; Gandhi, S. A smart nanosensor for the detection of human immunodeficiency virus and associated cardiovascular and arthritis diseases using functionalized graphene-based transistors. *Biosens. Bioelectron.* **2019**, *126*, 792−799.
(19) Aspermair, P.; Mishyn, V.; Bintinger, J.; Happy, H.; Bagga, K.; Subramanian, P.; Knoll, W.; Boukherroub, R.; Szunerits, S. Reduced graphene oxide-based field effect transistors for the detection of E7 protein of human papillomavirus in saliva. *Anal. Bioanal. Chem.* **2021**, *413*, 779−787.
(20) Vernick, S.; Trocchia, S. M.; Warren, S. B.; Young, E. F.; Bouilly, D.; Gonzalez, R. L.; Nuckolls, C.; Shepard, K. L. Electrostatic melting in a single-molecule field-effect transistor with applications in genomic identification. *Nat. Commun.* **2017**, *8*, 15450.
(21) Kwon, J.; Lee, Y.; Lee, T.; Ahn, J. H. Aptamer-Based Field-Effect Transistor for Detection of Avian Influenza Virus in Chicken Serum. *Anal. Chem.* **2020**, *92*, 5524−5531.
(22) Li, J.; Wu, D.; Yu, Y.; Li, T.; Li, K.; Xiao, M. M.; Li, Y.; Zhang, Z. Y.; Zhang, G. J. Rapid and unamplified identification of COVID-19 with morpholino-modified graphene field-effect transistor nanosensor. *Biosens. Bioelectron.* **2021**, *183*, 113206.
(23) East-Seletsky, A.; O'Connell, M. R.; Knight, S. C.; Burstein, D.; Cate, J. H.; Tjian, R.; Doudna, J. A. Two distinct RNase activities of CRISPR-C2c2 enable guide-RNA processing and RNA detection. *Nature* **2016**, *538*, 270−273.
(24) Hajian, R.; Balderston, S.; Tran, T.; deBoer, T.; Etienne, J.; Sandhu, M.; Wauford, N. A.; Chung, J. Y.; Nokes, J.; Athaiya, M.; Paredes, J.; Peytavi, R.; Goldsmith, B.; Murthy, N.; Conboy, I. M.; Aran, K. Detection of unamplified target genes via CRISPR-Cas9 immobilized on a graphene field-effect transistor. *Nat. Biomed. Eng.* **2019**, *3*, 427−437.
(25) Fu, X.; Shi, Y.; Peng, F.; Zhou, M.; Yin, Y.; Tan, Y.; Chen, M.; Yin, X.; Ke, G.; Zhang, X. B. Exploring the Trans-Cleavage Activity of CRISPR/Cas12a on Gold Nanoparticles for Stable and Sensitive Biosensing. *Anal. Chem.* **2021**, *93*, 4967−4974.
(26) Schroeder, A. B.; Dobson, E. T. A.; Rueden, C. T.; Tomancak, P.; Jug, F.; Eliceiri, K. W. The ImageJ ecosystem: Open-source software for image visualization, processing, and analysis. *Protein Sci.* **2021**, *30*, 234−249.
(27) Cai, B.; Huang, L.; Zhang, H.; Sun, Z.; Zhang, Z.; Zhang, G. J. Gold nanoparticles-decorated graphene field-effect transistor biosensor for femtomolar MicroRNA detection. *Biosens. Bioelectron.* **2015**, *74*, 329−334.
(28) Fozouni, P.; Son, S.; Díaz de León Derby, M.; Knott, G. J.; Gray, C. N.; D'Ambrosio, M. V.; Zhao, C.; Switz, N. A.; Kumar, G. R.; Stephens, S. I.; Boehm, D.; Tsou, C. L.; Shu, J.; Bhuiya, A.; Armstrong, M.; Harris, A. R.; Chen, P. Y.; Osterloh, J. M.; Meyer-Franke, A.; Joehnk, B.; et al. Amplification-free detection of SARS-CoV-2 with CRISPR-Cas13a and mobile phone microscopy. *Cell* **2021**, *184*, 323−333.
(29) Shan, Y. Y.; Zhou, X. M.; Huang, R.; Xing, D. High-Fidelity and Rapid Quantification of miRNA Combining crRNA Programmability and CRISPR/Cas13a trans-Cleavage Activity. *Anal. Chem.* **2019**, *91*, 5278−5285.
(30) Yue, H.; Shu, B.; Tian, T.; Xiong, E.; Huang, M.; Zhu, D.; Sun, J.; Liu, Q.; Wang, S.; Li, Y.; Zhou, X. Droplet Cas12a Assay Enables DNA Quantification from Unamplified Samples at the Single-Molecule Level. *Nano Lett.* **2021**, *21*, 4643−4653.
(31) Ravi, N.; Cortade, D. L.; Ng, E.; Wang, S. X. Diagnostics for SARS-CoV-2 detection: A comprehensive review of the FDA-EUA COVID-19 testing landscape. *Biosen. Bioelectron.* **2020**, *165*, 112454.
(32) Chevaliez, S. Strategies for the improvement of HCV testing and diagnosis. *Expert Rev. Anti. Infect. Ther.* **2019**, *17*, 341−347.
(33) Cacoub, P.; Comarmond, C. New insights into HCV-related rheumatologic disorders: A review. *J. Adv. Res.* **2017**, *8*, 89−97.
(34) WHOGlobal *Health Sector Strategy on Viral Hepatitis*, 2016-2021. Available from. https://www.afro.who.int/publications/global-health-sector-strategy-viral-hepatitis-2016-2021.
(35) Shi, S. T.; Lai, M. *HCV 5′ and 3′ UTR: When Translation Meets Replication. Hepatitis C Viruses: Genomes and Molecular Biology*; Tan, S. L., Ed.; Horizon Bioscience: Norfolk, 2006.
(36) Cai, B.; Wang, S.; Huang, L.; Ning, Y.; Zhang, Z.; Zhang, G. J. Ultrasensitive Label-Free Detection of PNA-DNA Hybridization by Reduced Graphene Oxide Field-Effect Transistor Biosensor. *ACS Nano* **2014**, *8*, 2632−2638.

https://doi.org/10.1021/acssensors.2c01200
ACS Sens. 2022, 7, 2680−2690